


Free energy and segregation dynamics of two channel-confined polymers of different lengthsJames M. Polson  and Qinxin Zhu**Department of Physics, University of Prince Edward Island, 550 University Avenue, Charlottetown, Prince Edward Island C1A 4P3, Canada* (Received 24 June 2020; revised 27 November 2020; accepted 4 January 2021; published 20 January 2021)

Polymers confined to a narrow channel are subject to strong entropic forces that tend to drive the molecules apart. In this study, we use Monte Carlo computer simulations to study the segregation behavior of two flexible hard-sphere polymers under confinement in a cylindrical channel. We focus on the effects of using polymers of different lengths. We measure the variation of the conformational free energy, F , with the center-of-mass separation distance, λ . The simulations reveal four different separation regimes, characterized by different scaling properties of the free energy with respect to the polymer lengths and the channel diameter, D . We propose a regime map in which the state of the system is determined by the values of the quantities N_2/N_1 and $\lambda/(N_1 + N_2)D^{-\beta}$, where N_1 and N_2 are the polymer lengths, and where $\beta \approx 0.64$. The observed scaling behavior of $F(\lambda)$ in each regime is in reasonable agreement with predictions using a simple theoretical model. In addition, we use MC dynamics simulations to study the segregation dynamics of initially overlapping polymers by measurement of the incremental mean first-passage time with respect to λ . For systems characterized by a wide range of λ in which a short polymer is nested within a longer one, the segregation dynamics are close to that expected for two noninteracting one-dimensional random walkers undergoing unbiased diffusion. When the free-energy gradient is large, segregation is rapid and characterized by out-of-equilibrium effects.

DOI: [10.1103/PhysRevE.103.012501](https://doi.org/10.1103/PhysRevE.103.012501)**I. INTRODUCTION**

The overlap of two polymer chains leads to a reduction in the total conformational entropy and thus an increase in the free energy. Often described as an “entropic force,” the gradient in the free energy tends to drive the polymers apart to reduce the loss in entropy [1,2]. When the polymers are confined to anisometric spaces with dimensions small compared to the bulk radius of gyration this interpolymer entropic repulsion is generally enhanced [3,4]. A notable example is polymer confinement in nanochannels, where the entropic force causes the polymers to segregate along the axis of the channel. This process has been the subject of numerous theoretical and computer simulation studies in recent years [4–23]. Most of these studies have examined the segregation behavior of flexible linear polymers [4–9,11,12,14,16,19,20], though some have also investigated the behavior of ring polymers [10,13,15,17,18,21]. In addition, the effects of bending rigidity [14,19], macromolecular crowding [15,18,21], and electrostatics [22,23] on the segregation dynamics and thermodynamics have been examined in detail.

A key motivation for theoretical studies of entropy-driven separation of confined polymers is to elucidate the role that entropy plays in the process of chromosome segregation in self-replicating bacteria [4,24–27]. Experiments have shown that the newly formed arms of a chromosome segregate as duplication proceeds while the terminus region remains at the

center of the nucleoid [28]. Modelling the chromosome as a polymer chain, Jun and Mulder showed that entropic demixing alone could account for such behavior [4]. Though some experimental studies have yielded results that are hard to reconcile with a purely entropic segregation mechanism [25,29–33], more recent studies have reported results consistent with this hypothesis [25,27,34–37]. Though a full understanding of the process is lacking [28] it appears likely that entropic forces contribute to driving segregation, perhaps in conjunction with other mechanisms [25,27,38].

Another motivation for theoretical studies of separation of confined polymers arises from recent advances in nanofluidic technology that facilitate the study *in vitro* of the physical behavior of multiple polymers confined to small spaces. A recent study by Capaldi *et al.* used fluorescence microscopy to study the dynamics and organization of two differentially stained λ -DNA molecules confined to rectangular nanocavities [39]. They also examined the confinement of a single λ -DNA molecule with a plasmid, which is a small circular DNA molecule typically found in bacteria outside the nucleoid. Such systems provide simple models of prokaryotic organisms that may help clarify the role of entropy as a demixing mechanism. They may also be useful for understanding the organization of multiple chromosomes inside a eukaryotic cell nucleus. In addition to contributing to understanding biological processes, insight provided by such experiments has important technological relevance. For example, the mixing or partitioning properties of multiple chains confined to channels or cavities may affect the performance of nanofluidic devices used for polymer manipulation and separation [40,41].

Our recent work on confinement effects of multiple-polymer systems has focused on the calculation of the overlap free energy of polymers inside channels and elongated cavities

*Present address: Department of Physics and Atmospheric Science, Sir James Dunn Building, 6310 Coburg Road, Halifax, Nova Scotia, Canada, B3H 4R2.

using Monte Carlo simulation methods [19,21]. Specifically, we have examined the variation of the free energy with respect to the polymer separation distance as well as other variables. Such free-energy functions are closely connected to the polymer mixing or segregation tendencies and the separation dynamics. As a measure of separation, we use the distance between the polymer centers of mass along the channel, in part because such a quantity is experimentally measurable [39]. Our goal has been to fully characterize these functions with respect to the key system parameters. These parameters include the confinement dimensions, polymer length, bending rigidity, the density of crowding agents, and the chain topology. We have shown that the scaling properties of the free-energy functions are reasonably consistent with predictions based on standard scaling theories in polymer physics. Thus far, we have considered only systems characterized by a high degree of symmetry, e.g., two identical linear or ring polymers confined to a cylindrical channel.

The purpose of the present study is to extend this work to examine the behavior of systems characterized by an asymmetry in the lengths of the polymers. This is expected to be relevant to the operation of nanofluidic devices for manipulation and analysis of DNA and other polymers. As in our other studies on this topic [19,21], we examine the behavior of two self-avoiding hard-sphere chains confined to a hard-walled channel. In addition to measuring and characterizing the free-energy functions, we also use MC dynamics simulations to investigate the segregation dynamics and interpret the results in light of the calculated free energies. The free-energy results are analyzed and interpreted using standard scaling theory methods. Generally, the results are in semiquantitative agreement with most predictions, though scaling exponents deviate slightly from theoretical values due to finite-size effects and deficiencies in the theoretical model. In addition, the segregation dynamics behavior align with expectations based on the equilibrium free-energy functions, though out-of-equilibrium effects are evident at separation distances corresponding to strong entropic forces.

II. MODEL

We examine a system of two flexible polymer chains confined to an infinitely long channel. Each polymer is modeled as freely jointed chain of hard spheres, where each spherical monomer has a diameter σ . The pair potential for nonbonded monomers is thus $u_{nb}(r) = \infty$ for $r \leq \sigma$, and $u_{nb}(r) = 0$ for $r > \sigma$, where r is the distance between the centers of the monomers. Pairs of bonded monomers interact with a potential $u_b(r) = 0$ if $0.9\sigma < r < 1.1\sigma$ and $u_b(r) = \infty$ otherwise. The polymer length is given in terms of the number of monomers of each polymer, N_1 and N_2 , where we choose $N_2 \leq N_1$.

The polymers are confined to a hard-wall cylindrical channel that is aligned along the z axis. The channel has an effective diameter D such that each monomer interacts with the wall of the tube with a potential $u_w(r) = 0$ for $r < D$ and $u_w(r) = \infty$ for $r > D$, where r is the distance of the monomer center from the central axis of the cylinder. Thus, D is the diameter of the cylindrical volume accessible to the centers

of the monomers, and the actual diameter of the cylinder is $D + \sigma$.

III. METHODS

In most simulations we measure the variation of the free energy with λ , the distance between the polymer centers of mass along the cylinder axis. We employ Monte Carlo simulations with the Metropolis algorithm together with the self-consistent histogram (SCH) method [42]. To implement the SCH method, we carry out many independent simulations, each of which employs a unique “window potential” of the form:

$$W_i(\lambda) = \begin{cases} \infty, & \lambda < \lambda_i^{\min} \\ 0, & \lambda_i^{\min} < \lambda < \lambda_i^{\max} \\ \infty, & \lambda > \lambda_i^{\max} \end{cases}, \quad (1)$$

where λ_i^{\min} and λ_i^{\max} are the limits that define the range of λ for the i th window. Within each window of λ , a probability distribution $p_i(\lambda)$ is calculated in the simulation. The window potential width, $\Delta\lambda \equiv \lambda_i^{\max} - \lambda_i^{\min}$, is chosen to be sufficiently small that the variation in F does not exceed a few $k_B T$. The windows are chosen to overlap with half of the adjacent window, such that $\lambda_i^{\max} = \lambda_{i+2}^{\min}$. The window width was typically in the range $\Delta\lambda = 2\sigma - 4\sigma$. The SCH algorithm was employed to reconstruct the unbiased distribution, $\mathcal{P}(\lambda)$, from the $p_i(\lambda)$ histograms. The free energy follows from the relation $F(\lambda) = -k_B T \ln \mathcal{P}(\lambda) + \text{const}$. We choose the constant such that $F(\lambda = \infty) = 0$.

In some simulations we consider polymers with centers of mass that overlap along the channel and measure the variation of the free energy with $\zeta \equiv X_1 - X_2$, where ζ is the difference in the spans of the two polymers along the channel, X_1 and X_2 . The SCH method is implemented for ζ in exactly the same manner as for λ . Specifically, we use window potentials of the form of Eq. (1) for ζ such that trial MC moves that yield values of ζ outside the range of the window are rejected. The resulting collection of probability distributions $p_i(\zeta)$ are used with the SCH algorithm to reconstruct the underlying distribution $\mathcal{P}(\zeta)$ that yields the free energy, $F(\zeta) = -k_B T \ln \mathcal{P}(\zeta)$.

Polymer configurations were generated by carrying out single-monomer moves using a combination of translational displacements and crankshaft rotations. In addition, whole-polymer displacements and reptation moves of each polymer along the channel axis were also employed to increase the efficiency of sampling $p_i(\lambda)$. Each trial move was rejected if it resulted in overlap between particles or between a particle and a confinement surface or if it led to a violation of the bonding constraints; otherwise it was accepted. Measurements of the various quantities were carried out every 100 MC cycles over a run time whose duration was $\mathcal{O}(10^7 - 10^8)$ MC cycles. A single MC cycle corresponds to attempting each of the following coordinate changes once, on average: (1) movement of a single randomly chosen monomer by translation or crankshaft rotation, (2) whole-polymer displacement of a randomly selected polymer along the channel by changing all the z coordinates by the same random value, and (3) reptation at a randomly chosen end of a randomly selected polymer. After initializing the particle positions, the simulation

proceeded through an equilibration period prior to sampling data. Since the polymer configurations were initially chosen for convenience to be linear and aligned along the channel, such an equilibration period is necessary for the system to relax out of this highly artificial initial state. As an illustration, for two identical polymers of length $N_1 = N_2 = 300$ in a $D = 6$ cylindrical channel, the system was equilibrated for 1×10^7 MC cycles, following which a production run of 4×10^7 MC cycles was carried out. Equilibration and production run times were typically chosen to be greater for longer polymer systems.

In addition to free-energy calculations, Monte Carlo dynamics simulations were used to study the segregation dynamics of the two confined polymers. The MC dynamics method is chosen here since the Langevin dynamics method is inapplicable to molecular models with discontinuous potentials. Provided the random trial moves are local and do not lead to chain crossing, the random motions of individual monomers can be viewed as discretized realizations of a stochastic dynamical process such as that described by a Langevin equation [43]. Consequently, for this model diffusion obeys Rouse scaling of the diffusion coefficient, i.e., $D \propto 1/N$. Though MC dynamics does not provide an absolute timescale or enable probing the short-time dynamical behavior such as bond vibration, it can be effective in determining scaling exponents associated with polymer dynamics on longer time scales [44]. As in Ref. [19] we choose to simulate polymer motion solely through random monomer displacement. The coordinates of a randomly chosen monomer were displaced by an amount Δr_α for $\alpha = x, y, z$. Each coordinate displacement was randomly chosen from a uniform distribution in the range $[-0.14\sigma, 0.14\sigma]$. The acceptance criteria are the same as described above for the free-energy calculations, with the exception that the potential of Eq. (1) is not applied. The range chosen for the distribution of the single-monomer trial displacements yields acceptance ratios slightly below 50%, corresponding to efficient sampling of configurations during the simulation. In effect, this choice also calibrates the timescale. The polymer configurations were initially constrained to $\lambda = 0$ while the polymer chains were equilibrated. Following equilibration, the constraint was removed and the polymers underwent segregation along the channel. The main quantity we measure is the incremental mean first-passage time (IMFPT), τ , defined as the first time the polymers are separated by a given value of λ . The IMFPT was originally introduced to characterize dynamics in polymer translocation simulations [45,46]. During the segregation process we measure the degree of overlap of the polymers as well as their extension lengths. We simulated typically 100–200 segregation events to calculate averages of these quantities.

For both the free-energy calculations and the MC dynamics simulations we calculate the mean extension lengths, X_1 and X_2 , of each polymer along the channel. We also measure the mean overlap distance L_{ov} , which is the range of positions along the channel occupied by part of the contours of both chains. These quantities are illustrated in Fig. 1, which shows a snapshot of a system of two partially overlapping polymers. Note that L_{ov} is more generally defined as follows. With reference to the illustration in Fig. 1, it is the difference between the z coordinate of the rightmost monomer of the

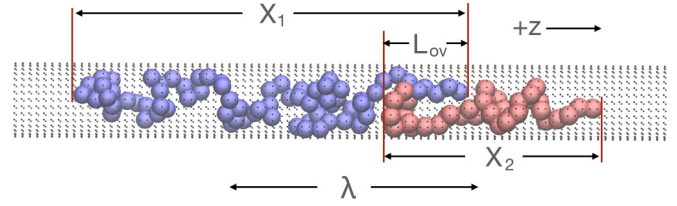


FIG. 1. Snapshot of two polymers with lengths $N_1 = 80$ and $N_2 = 40$ in a cylindrical tube of diameter $D = 4$. The polymer extension lengths, X_1 and X_2 , the overlap distance, L_{ov} , and the distance between polymer centers of mass, λ , are each labeled in the figure.

longer (blue) polymer and the leftmost monomer of the shorter (red) polymer. Clearly, when the polymers overlap, L_{ov} is the overlap distance shown in the figure. However, if the polymers do not overlap, then $L_{ov} < 0$, and its magnitude is simply the distance along the z axis between the nearest pair monomers, one on each polymer.

In the results presented below, distances are measured in units of σ , energy is measured in units of $k_B T$, and time is measured in MC cycles.

IV. RESULTS

A. General features of the free-energy functions

Let us first examine the general qualitative features of the free-energy functions. As an illustration, Fig. 2 shows the variation of the free energy with respect to the center-of-mass distance λ for polymers of length $N_1 = 400$ and $N_2 = 200$ confined to a channel of diameter $D = 4$. The graph also shows the variation of the extension lengths, X_1 and X_2 , as well as the overlap distance, L_{ov} , with λ . Four different regimes are labeled, each corresponding to a physically distinct state.

In regime I at low center-of-mass separation ($\lambda \lesssim 50$), the free energy and the overlap and extension lengths are all constant with respect to λ . This regime corresponds to the “nesting” of the shorter polymer within the longer polymer.

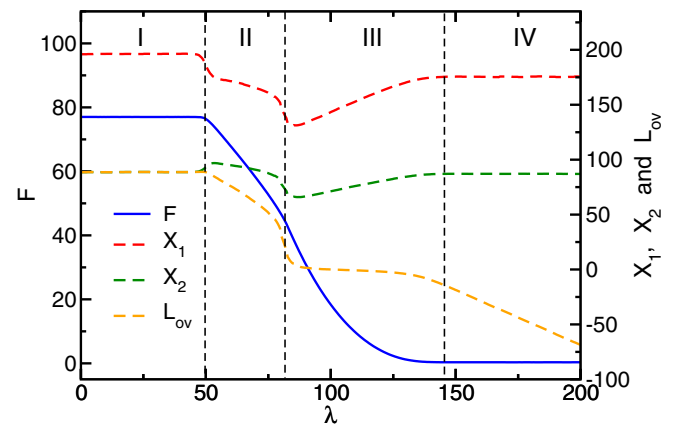


FIG. 2. Free energy vs λ for polymers of length $N_1 = 400$ and $N_2 = 200$ confined to a cylinder of diameter $D = 4$. Overlaid on the graph are the extension lengths of the polymers, X_1 and X_2 , as well as the overlap distance, L_{ov} , as defined in the text. The vertical dashed lines denote approximate boundaries of the four regimes described in the text.

In this case, changing the center-of-mass distance changes neither extension length nor the overlap length (which is equal to X_2). At $\lambda \approx 50$, the system undergoes a transition to regime II, which is characterized by a drop in F . At the transition, the extension of the longer polymer abruptly decreases at the transition while that for the shorter polymer slightly increases. This regime corresponds to partial overlap of the polymers along the channel (as illustrated in Fig. 1). As λ decreases, the overlap distance decreases, as does each of the extension lengths.

At $\lambda \approx 80$, the system undergoes transition into regime III, where the curvature of $F(\lambda)$ changes from positive to negative. Significantly, the polymers have essentially no longitudinal overlap ($L_{ov} \approx 0$), and the extension lengths each increase with λ . This regime corresponds to nonoverlapping polymers that are longitudinally compressed and pressed against each other. Varying λ controls the degree of compression of the chains, each of which behaves like an entropic spring with a free energy that rises rapidly with increasing compression.

At $\lambda \approx 145$ the system undergoes a final transition to regime IV, which corresponds to no physical contact between the polymers. L_{ov} becomes increasingly negative with λ , indicating a growing space between the polymers. As expected, the extension lengths and the free energy are invariant with respect to λ here. Qualitatively similar behavior for all four regimes was observed for polymers of equal length in Ref. [21], where it is described and explained in greater detail. The key differences here are a wider nesting regime, unequal values of X_1 and X_2 , and a slight increase in X_2 at the I-II regime boundary.

B. Nesting regime

Let us now examine regime I in detail. In this regime, the centers of mass are close enough that the shorter polymer is completely nested within the longer polymer. (Note: An exception to this rule occurs when the polymer lengths differ by only a small amount, as will be discussed in Sec. IV C.) In addition, the free energy is constant and equal to the value of the free-energy barrier height, which we define $\Delta F \equiv F(\lambda = 0) - F(\lambda = \infty)$. Since we choose $F(\infty) = 0$, it follows that $\Delta F = F(\lambda = 0)$. Figure 3(a) shows the scaling of ΔF with N_2 for fixed $N_1 = 300$ and for various channel diameters. In each case, ΔF increases linearly with N_2 , and the slope of the linear functions increases with decreasing D . Figure 3(b) shows the variation of ΔF with D for fixed $N_1 = 300$ and for $N_2 = 50-300$. For arbitrary N_2 , we find that $\Delta F \sim D^{-\alpha}$, where α is in the narrow range of $\alpha \approx 1.81-1.84$ for all cases except $N_2 = 50$. Consequently, the λ -invariant free energy in regime I scales as $F \propto N_2 D^{-\alpha}$, where $\alpha \approx 1.82$.

Let m_1 and m_2 be the average number of monomers that lie in the overlap range for any separation λ . Figure 4(a) shows variation of m_1 and m_2 with λ for a case where $N_1 = 300$, $N_2 = 200$, and $D = 6$. In the case of partial overlap in regime II, we see that $m_1 \approx m_2$ and that both increase as the separation decreases. On further decreasing λ , the system enters regime I, and the values of m_1 and m_2 diverge. Since the shorter polymer is now completely nested inside the longer polymer, it follows that $m_2 = N_2 = 200$. On the other hand,

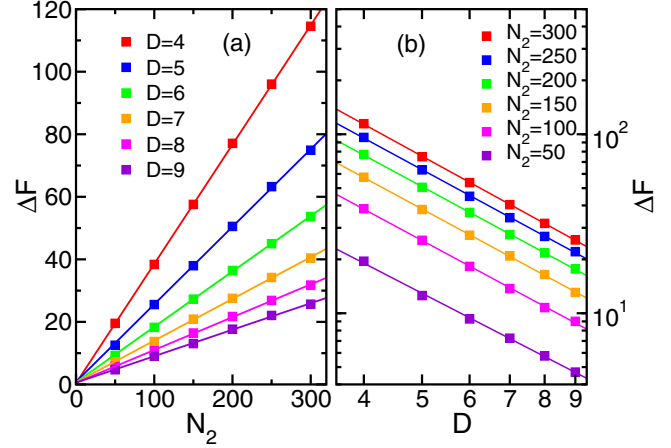


FIG. 3. (a) Free-energy difference ΔF vs polymer length N_2 for two polymers for the case of $N_1 = 200$. Results for various channel diameters are shown. The solid lines show fits to a linear function. (b) $\Delta F \equiv F(\lambda = 0) - F(\lambda = \infty)$ vs channel diameter D for two polymers of length $N_1 = 200$ and N_2 confined to an infinitely long cylindrical channel. Results are shown for various values of N_2 . The solid lines show fits to a power law $\Delta F \sim D^{-\beta}$. The best-fit scaling exponents are $\beta = 1.84 \pm 0.01$ for $N_2 = 300$, $\beta = 1.82 \pm 0.02$ for $N_2 = 250$, $\beta = 1.81 \pm 0.01$ for $N_2 = 200$, $\beta = 1.81 \pm 0.01$ for $N_2 = 150$, $\beta = 1.81 \pm 0.02$ for $N_2 = 100$, and $\beta = 1.73 \pm 0.03$ for $N_2 = 50$.

number of monomers from the longer polymer in the overlap region abruptly decreases to a constant value that satisfies $m_1 < m_2$. The inset of Fig. 4(a) shows that both the value of m_1 as well as the overlap distance L_{ov} both increase linearly with increasing N_2 . The exception is the limiting case where $N_2 = N_1 = 300$.

Figure 4(b) shows the variation of L_{ov} and m_1 with D in regime I for the case where $N_1 = 300$ and $N_2 = 200$. In both cases, power-law scaling is observed. The overlap distance scales as $L_{ov} \sim D^{-0.75}$, while m_1 has a much weaker dependence on D , with a scaling of $m_1 \sim D^{-0.175}$.

To understand the scaling behavior of Figs. 3 and 4 we use a simple theoretical model that is based on two approximations. First, the scaling behavior of the free energy is assumed to correspond to the predictions of the blob model in the de Gennes confinement regime [47]. A second approximation is that introduced by Jung *et al.* to approximate the free energy of overlapping confined chains [10]. In this picture, the effect of longitudinal overlap on the conformational behavior of the two channel-confined polymers is approximately the same as that of confining the overlapping portions of the chains to virtual tubes of reduced cross-sectional areas. The overlapping portion of polymer 1 is pictured as confined to a virtual tube of diameter $D_1 = D\sqrt{\xi}$, where $\xi < 1$, while the overlapping portion of polymer 2 is likewise confined to a virtual tube of diameter $D_2 = D\sqrt{\xi_0 - \xi}$. Jung *et al.* used this model to describe the conformational behavior of a ring polymer confined to a channel. Since the ring polymer was modeled as two completely overlapping linear polymers of equal length, $D_1 = D_2$. Neglecting lateral interpenetration requires the cross-sectional areas of the virtual tubes sum to equal that of the actual channel. Together, these assumptions

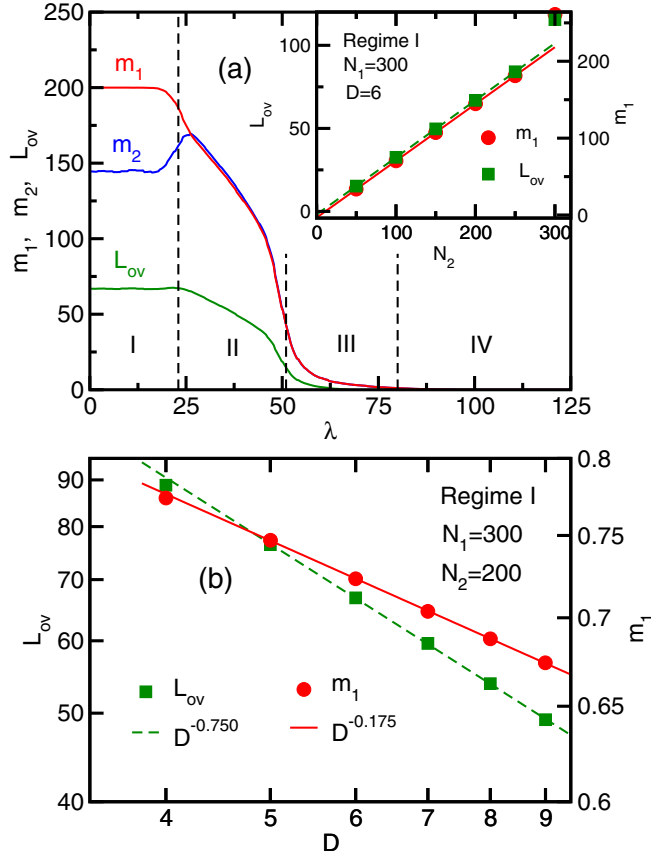


FIG. 4. (a) Variation of m_1 , m_2 , and L_{ov} with λ for a system with $N_1 = 300$, $N_2 = 200$, and $D = 6$. As noted in the text, m_1 and m_2 are the mean number of monomers of each polymer that lie in the overlap region. The dashed lines denote the approximate boundaries of the four overlap regimes. The inset shows the variation of m_1 and L_{ov} with N_2 for fixed $N_1 = 300$ and $D = 6$. (b) Variation of L_{ov} and m_1 with channel diameter for the case where $N_1 = 300$, $N_2 = 200$. The solid lines are fits to power laws.

imply that $\xi = \frac{1}{2}$ and $\xi_0 = 1$. Choosing $\xi_0 \geq 1$ effectively allows for some lateral interpenetration, while $\xi_0 - \xi \neq \xi$ (i.e., $D_1 \neq D_2$) allows for unequal virtual tube sizes, which is clearly required for regime I, where $m_1 \neq m_2$. Note that ξ and ξ_0 are assumed to be independent of D .

In Appendix A we show that this theoretical model predicts that the free-energy barrier height scales as

$$\Delta F \propto N_2 D^{-1/\nu} f(m_1/N_2; \xi_0), \quad (2)$$

where $f(m_1/N_2; \xi_0)$ is defined in Eq. (A7). Thus, the model correctly predicts the linear scaling of ΔF with respect to N_2 observed in Fig. 3(a). The model also predicts that $\Delta F \sim D^{-1.70}$, where we use the Flory exponent value $\nu \approx 0.588$. Thus, the predicted scaling exponent is close to measured exponent of ≈ 1.82 obtained from fits to the data in Fig. 3(b). A similar discrepancy was observed for equal-length linear and ring polymers in our previous study [21].

The origin of the discrepancy between the values of the measured and predicted scaling exponent is likely a combination of two factors. The first is a breakdown in the blob-model scaling behavior for the narrow channel widths and polymer

lengths considered here. As noted in Ref. [48] such scaling requires that D and N be sufficiently large that both the number of monomers per blob, $g \sim D^{1/\nu}$, and the number of blobs, $n_{\text{blob}} = N/g$, be large compared to unity. A second factor is a breakdown in the validity of the approximation used to estimate the overlap free-energy function in Eq. (2). The accuracy of this approximation was measured directly in Ref. [21], and the simulations revealed quantitative inaccuracies arising from finite-size effects. Additional insight into this discrepancy is provided by Eq. (A8) in Appendix A, where the theory predicts that m_1 should be independent of the channel width. This contradicts the results in Fig. 4(b), which shows a weak but nonnegligible dependence of m_1 on D . In addition, the overlap length is predicted to scale as $L_{ov} = X_2 \propto N_2 D_2^{(\nu-1)/\nu} = N_2 (D \sqrt{\xi_0 - \xi})^{(\nu-1)/\nu} \propto D^{-0.70}$. The predicted scaling exponent is close to the value measured from the data in Fig. 4(b), though once again the discrepancy is nonnegligible.

We suspect that the difference between the predicted and measured scaling exponents arises from the assumption that the factors ξ and ξ_0 are independent of D . While incorporation of such a dependence could improve the theory, there are no obvious physical arguments to suggest any particular functional form. Despite these limitations, the reasonably accurate predictions suggest that the theoretical model provides a decent understanding of the overlap free-energy scaling behavior. Calculations presented in Ref. [21] suggest that using constant values of the quantities ξ and ξ_0 may be justified but only in the limit of much larger N and D . As noted in that study, no single value of the rescaling factor yields predictions of high quality for the polymer lengths and channel width employed here [21].

C. Nesting free-energy function for $\lambda = 0$

Let us consider further the system behavior in the nesting regime in the case of overlapping centers of mass, i.e., $\lambda = 0$. This state was examined in detail by Minina and Arnold [16,17] for the case of two polymers of equal length. They noted that the separation kinetics of polymers that begin at $\lambda = 0$ show an initial lag time, which they attributed to a free-energy barrier associated with the nesting of one polymer within the other. We examined the scaling behavior of this free-energy barrier previously for two identical polymers [21]. Here we extend that study and examine the effects of small differences in the lengths of the polymers on the barrier.

Following Ref. [21] we calculate the free energy at $\lambda = 0$ as a function of $\zeta \equiv X_1 - X_2$, i.e., the difference in the extension lengths of the polymers. When $N_1 = N_2$, it is equally likely that either polymer is nested inside the other. Consequently, two identical free-energy minima are observed separated by a small free-energy barrier [16,17,21]. Such a symmetric free-energy function is shown in Fig. 5(a) in the case of $N_1 = N_2 = 200$ for $D = 4$. As N_2 is decreased to values below N_1 , the double-well structure is initially preserved, though the free energy at the minimum at lower ζ tends to increase relative to the minimum at higher ζ . Thus, provided N_2 is not too much less than N_1 , the longer polymer nested inside the shorter polymer represents a metastable state separated from the global free-energy minimum (where the

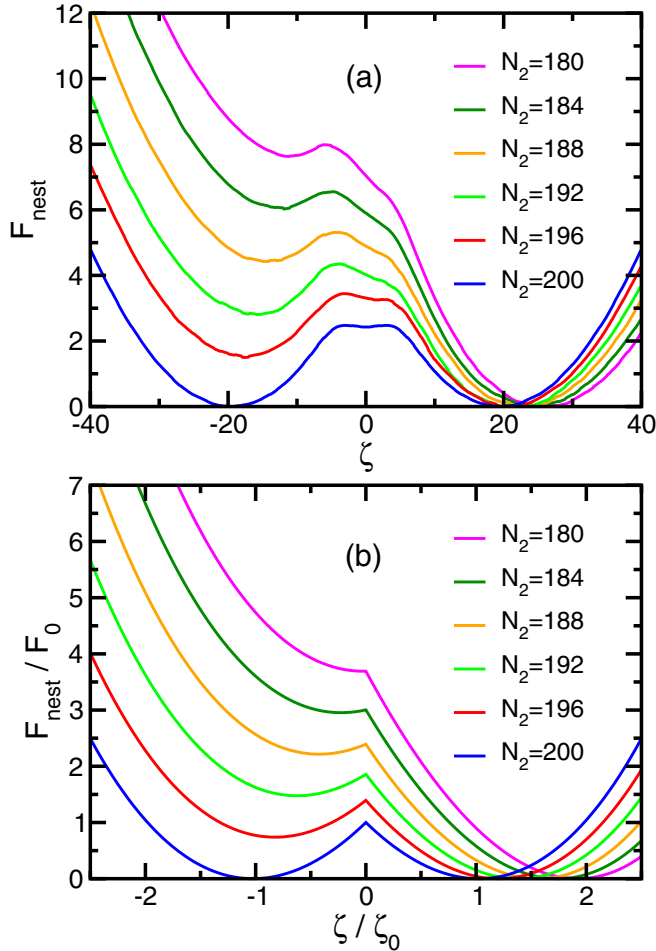


FIG. 5. (a) Free energy vs extension length difference $\zeta \equiv X_1 - X_2$ for polymers with overlapping centers of mass. Results are shown for $D = 4$, $N_1 = 200$ and for various values of N_2 . (b) Prediction of the nesting free energy using the theory developed in Appendix A. The scaling factors for the axes are defined with respect to the curve for $N_1 = N_2 = 200$: (i) $F_0 \equiv F_{\text{nest}}(0)$ and (ii) ζ_0 is the value of ζ at the right minimum of F_{nest} .

roles of the polymers are reversed) by a free-energy barrier. The height of the barrier decreases with decreasing N_2 until it almost disappears at $N_2 = 180$.

Some understanding of the origins of the trends observed in Fig. 5(a) is provided by the theoretical model developed by Minina and Arnold [16,17]. They employed essentially the same two approximations as were used to elucidate the scaling behavior observed in Fig. 3 above: (i) using the de Gennes blob model to describe the scaling of the free energy and extension lengths of channel-confined polymers and (ii) assuming that the effect of overlap on the free energy is the same as that of separately confining each polymer to a different virtual tube, the sum of whose cross-sectional areas is equal to that of the real channel [10]. In Appendix B we modify their theory to accommodate polymers of unequal length. The theoretical predictions are shown in Fig. 5(b). As the theory employs scaling relations with undetermined prefactors, the axes have been scaled by factors as defined in the caption to avoid confusion. Although the shape of the

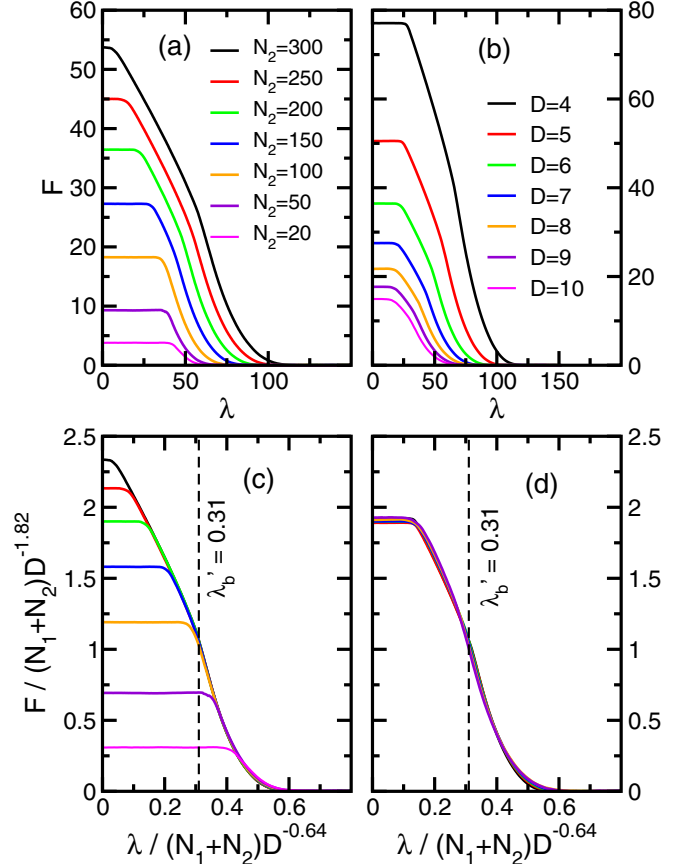


FIG. 6. (a) Free energy vs λ for polymers confined to a cylinder of diameter $D = 6$. One polymer length is fixed to $N_1 = 200$. Results for various values of the polymer length $N_2 (\leq N_1)$ are shown. (b) F vs λ for polymers of length $N_1 = 300$ and $N_2 = 200$ for various cylinder diameters. (c) $F' \equiv F / (N_1 + N_2) D^{-1.82}$ vs $\lambda' \equiv \lambda / (N_1 + N_2) D^{-0.64}$ using the data in panel (a). (d) As in (c) except using the data in panel (b). The vertical dashed lines in panels (c) and (d) mark the approximate boundary at $\lambda'_b \approx 0.31$ between regimes II and III for $N_2 \gtrsim 100$.

free-energy barrier is poorly described by the theory, the key qualitative behavior is well reproduced. In particular, as the length asymmetry increases (i.e., N_2 decreases while N_1 is held fixed), the position of the free-energy minima both shift to higher ζ , and the free energy of the negative- ζ minimum increases relative to that of the positive- ζ minimum. In addition, the metastable state eventually disappears as N_2 decreases. As before, quantitative discrepancies arise from the nature of the approximations employed.

D. Scaling behavior of $F(\lambda)$

Thus far we have focused on the behavior of the system solely in regime I. We now examine the scaling properties of $F(\lambda)$ over the full range of λ across all regimes. Figure 6(a) shows free-energy functions for $N_1 = 300$ and $D = 6$ and for various values of the length N_2 . The linear increase of ΔF with N_2 has already been discussed at length in Sec. IV B. The increasing width of the free-energy barrier with increasing N_2 can be understood as follows. In the case of isolated polymers

with large λ , the extension lengths are each proportional to the contour length. Thus, as the polymers are brought closer together, the center-of-mass distance λ corresponding to the point where the polymers make contact (i.e., at the boundary of regime III and IV) is shorter for smaller N_2 . Another trend is the decreasing width of regime I as N_2 increases and approaches N_1 . To understand this trend, we note that the transition to regime II occurs at the value of λ where the location of the nested polymer's left (right) boundary along the channel reaches the left (right) boundary of the longer polymer. This occurs when $\lambda = (X_1 - X_2)/2 = (X_1 - c_2 N_2)/2$, since $X_2 \propto N_2$ in the nesting regime and where c_2 is the proportionality constant. Thus, the value of λ at this transition decreases with increasing N_2 , thereby reducing the width of regime I. Finally, the boundary between regimes II and III evident from the inflection point in the functions disappears for $N_2 \lesssim 100$.

Figure 6(b) shows free-energy functions for $N_1 = 300$ and $N_1 = 200$ for various values of the cylinder diameter D . As D increases, we note that the barrier height and width both decrease. The latter trend is due to the fact that reducing the confining tube width also reduces the extension of the polymers. Consequently, the polymer center-of-mass separation distance at the II-III and III-IV regime boundaries is smaller for larger D .

The quantitative nature of the scaling of $F(\lambda)$ with respect to N_2 and D can be elucidated by considering the scaled variables $F' \equiv F/(N_1 + N_2)D^{-\alpha}$ and $\lambda' \equiv \lambda/(N_1 + N_2)D^{-\beta}$. Figures 6(c) and 6(d) show the results such a transformation on the free-energy functions of Figs. 6(a) and 6(b), respectively, using exponents of $\alpha = 1.82$ and $\beta = 0.64$. The results are revealing. In Fig. 6(c), all of the functions for the various values of N_2 collapse to a universal curve, except at low λ' , where the system is in regime I. The universal curve can be defined as the function for $N_1 = N_2$. Define λ'_b to be the value of λ' at the boundary between regimes II and III for this curve. Clearly, the boundary is at $\lambda'_b \approx 0.31$, and is marked on the graph with a dashed line. Now define λ'_* as the value of λ' at which the regime-I plateau meets the universal curve. We see that λ'_* increases as the polymer length N_2 decreases. In the case where $N_2 \gtrsim 100$, $\lambda'_* < \lambda'_b$, which simply implies that regime II exists for this range of N_2 . On the other hand, for $N_2 \lesssim 100$, $\lambda'_* > \lambda'_b$. This means that regime II is absent for these shorter polymer lengths, and thus the system passes directly from the nesting regime (I) to the compressed regime (III). In Fig. 6(d), all of the scaled free-energy functions for different D and fixed N_2 collapse to a universal curve in all regimes, including regime I.

The results above suggest the following scaling for the free energy for regimes II, III, and IV:

$$F(\lambda) = (N_1 + N_2)D^{-\alpha} f(\lambda/(N_1 + N_2)D^{-\beta}), \quad (3)$$

where $f()$ is a universal function and where $\alpha \approx 0.64$ and $\beta \approx 1.82$. (Since $F = 0$ in regime IV, the scaling is automatically satisfied here.) This is consistent with the case of symmetric systems with $N_1 = N_2 \equiv N$, for which we previously showed that $F(\lambda) = ND^{-\alpha} f(\lambda/ND^\beta)$ with approximately equal exponent values [21]. In the case of regime I, we have already noted in Sec. IV B that F is independent of λ and scales as

$$F \propto N_2 D^{-\alpha}. \quad (4)$$

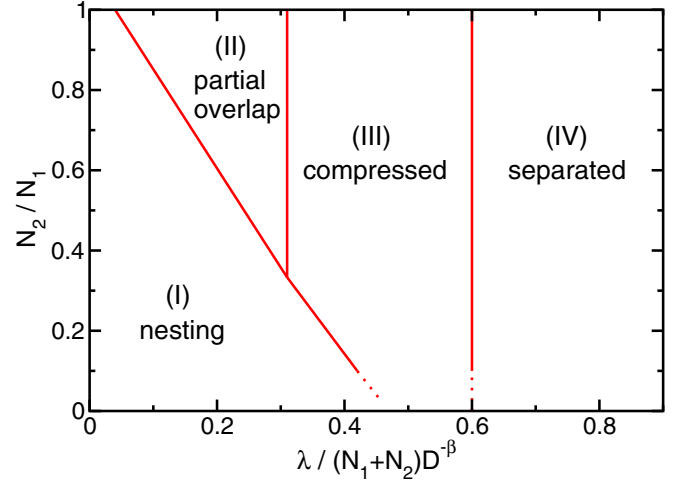


FIG. 7. Proposed regime map for two polymers of length N_1 and N_2 ($\leq N_1$) separated by center-of-mass distance λ confined to a cylindrical channel of diameter D . The II-III and III-IV phase boundaries are vertical lines, as shown. However, the I-II and I-III boundaries are only qualitatively illustrated. Simulations with $N_1 = 300$ yield an exponent of $\beta \approx 0.64$. In regimes II, III, and IV, the free-energy functions scale according to Eq. (3), and in regime I the free energy satisfies Eq. (4).

For $N_1 = 300$ and $N_2 = 200$ the fit to the data in Fig. 3(b) yielded $\alpha \approx 1.84$, which is very close to the value of $\alpha = 1.82$ that best collapses the curves in Fig. 6(d). Although the scaling relations were obtained from analysis of data for $N_1 = 300$, the results do not change for other values of N_1 . In Appendix C, this is illustrated by a comparison of free-energy functions calculated for $N_1 = 200, 300$, and 400 . The boundary between regimes I and II and the boundary between regimes I and III are determined by the condition the free energy in Eqs. (3) and (4) are equal. This leads to the condition that $f(\lambda') \propto (1 + (N_2/N_1)^{-1})^{-1}$, where $\lambda' \equiv \lambda/(N_1 + N_2)D^{-\beta}$ and where the proportionality constant is the same as in Eq. (4). Thus, the I-II and I-III regime boundaries are uniquely determined by the quantities λ' and N_2/N_1 , as implicitly true in Eq. (3) for the II-III and III-IV boundaries.

Figure 7 shows a “phase diagram” illustrating the approximate boundaries separating the four scaling regimes. Our previous study [21] covered the special case of $N_2/N_1 = 1$, which corresponds to a horizontal line at the very top of this diagram. Clearly, the present study extends the characterization of the system to cover a much larger region of parameter space. Of special note is the disappearance of the partial overlapping regime for $N_2/N_1 \lesssim 0.3$, i.e., for a sufficiently large polymer size asymmetry. This behavior has a simple analog in the phase behavior of substances like CO_2 or water, i.e., the disappearance of a liquid phase on heating a solid at a fixed pressure below that of the triple-point pressure so that the solid sublimates directly to a gas.

In order to understand the regime map of the system described above, we follow an approach similar to that in our previous study [21]. Since we have already explained the scaling of regime I in Sec. IV B, and since the scaling of $F = 0$ in regime IV follows Eq. (3) trivially, we need only

deal with regimes II and III. We begin with the latter. Recall that regime III corresponds to the case where the polymers are compressed and in contact, but not overlapping. Here the two polymers behave much like a single channel-confined polymer in a compressed state. Employing the renormalized Flory theory of Jun *et al.* [49], the free energy for a single linear polymer of length L_{ext} is

$$F = AL_{\text{ext}}^2/(N/g)D^2 + BD(N/g)^2/L_{\text{ext}}, \quad (5)$$

where A and B are constants of order unity and $g \sim D^{1/\nu}$ is the number of monomers in a compression blob of diameter D . Noting $\lambda = L_{\text{ext}}/2$ (i.e., assuming uniform compression) it is easily shown that

$$F(\lambda) = (N_1 + N_2)D^{-1/\nu} w[\lambda/(N_1 + N_2)D^{1-1/\nu}], \quad (6)$$

where $w(x) = 4Ax^2 + B/2x$. This is consistent in form with the scaling of Eq. (3), with scaling exponents of $\alpha = 1/\nu$ and $\beta = 1/\nu - 1$. Using $\nu = 0.588$, this corresponds to a prediction of $\alpha = 1.70$ and $\beta = 0.70$, which are close to the measured values of $\alpha = 1.82$ and $\beta = 0.64$.

To understand the scaling of $F(\lambda)$ in regime II, we use the same theoretical models developed in Appendices A and B to understand the scaling of the free-energy barrier height. Specifically, we employ the blob scaling model together with the approximation introduced by Jung *et al.* [10] to account for the conformational behavior of overlapping chains in channels. The calculation is presented in Appendix D. In Eq. (D4), we find that $F/(N_1 + N_2)D^{-1/\nu} \propto m/(N_1 + N_2)$, where $m \equiv m_1 = m_2$ is the number of overlapping monomers per polymer. In order for Eq. (3) to be satisfied in regime II, we expect $m/(N_1 + N_2)$ to be a universal function of $\lambda/(N_1 + N_2)D^{1-1/\nu}$ independent of the values of N_1 and N_2 . As described in the Appendix, the observed variation of $m/(N_1 + N_2)$ with $\lambda/(N_1 + N_2)D^{1-1/\nu}$ does show some slight dependence on N_2 and N_1 (though not on D), but this appears to be negligible over the range of λ corresponding to regime II. As for regime III the scaling exponents for Eq. (3) are predicted to be $\alpha = 1/\nu \approx 1.70$ and $\beta = 1/\nu - 1 \approx 0.70$. Again, the deviations between the predicted and measured exponents arise from the nature of the approximations used.

E. Segregation dynamics

We now consider the dynamics of polymers segregating from an initial state of maximum overlap at $\lambda = 0$. Several other simulation studies have investigated the segregation dynamics of comparable systems. In the present work, our goal is to elucidate the relationship, if any, between the dynamics and the equilibrium free-energy functions. This extends the range of calculations carried out in our previous study [19], which considered only the case of polymers of equal length.

Figure 8(a) shows the variation of the IMFPT with λ for the case of segregating polymers. Results are shown for a confinement tube diameter of $D = 4$, $N_1 = 200$ and for various values of N_2 . As a useful reference, Fig. 8(b) shows the free-energy functions for each of the systems considered in Fig. 8(a). At low λ , we find that τ obeys a power law of the form $\tau \sim \lambda^\mu$, where $\mu \approx 2.1$. This dynamical regime approximately corresponds to regime I of the free-energy functions, i.e., the regime in which F is invariant with

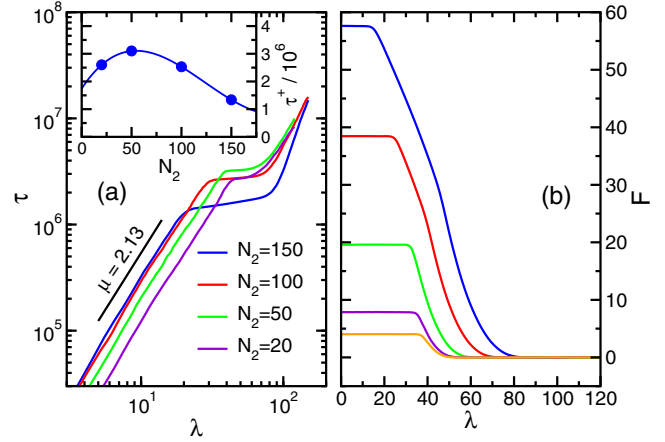


FIG. 8. (a) Incremental mean-first-passage time τ vs λ for segregating polymers. Results are shown for $D = 4$, $N_1 = 200$ and for various values of N_2 . The inset shows the variation of τ^\dagger with λ , where τ^\dagger is the mean first-passage time for the system to enter the middle dynamical regime, as explained in the text. (b) Free energy functions for the systems described in (a).

respect to λ . In addition, at any separation distance λ in this regime τ increases with increasing N_2 . A simple explanation for these trends follows from modeling the polymers as two independent 1D random walkers with diffusion coefficients \mathcal{D}_1 and \mathcal{D}_2 . In this case, the distance between the two walkers satisfies a diffusion equation with effective diffusion coefficient $\mathcal{D}_{\text{eff}} = \mathcal{D}_1 + \mathcal{D}_2$. Starting from a separation $\lambda_0 = 0$, the first-passage time required to reach a separation of $\pm\lambda$ for this simple diffusion is $\tau = \lambda^2/[24(\mathcal{D}_1 + \mathcal{D}_2)]$ [50]. Thus, the noninteracting-walkers model predicts an exponent of $\mu = 2$, which is close to the observed value. Since $\mathcal{D}_2 \propto 1/N_2$, it follows that τ will increase as the N_2 increases, consistent with the results.

The variation of τ with separation distance changes abruptly at a N_2 -dependent value of λ after which it increases at a much slower rate. Following this stage, there is a second transition at a higher value of λ , after which τ increases rapidly once more with separation distance. The middle regime corresponds roughly to regimes II and III of the free-energy functions. Thus, it corresponds to the region in which the short polymer has left the nested stage and is either partially overlapping with the long polymer or else is not overlapping but is in contact and compressed. Significantly, these regimes correspond to the rapid decrease in the free energy. The gradient of F can be considered an effective force that drives the polymers apart. While the system is subject to this effective force, any additional increase in the separation distance is achieved in much less time than is the case in its absence, leading to the observed behavior. Once the polymers are no longer in contact (i.e., regime IV) the separation dynamics are once again governed by the much slower process of unbiased diffusion, resulting in a more rapid increase in τ with λ .

Another interesting trend is the variation of τ with the length of the short polymer, N_2 , in the middle dynamical regime. Unlike the case at low λ where τ increases monotonically with N_2 , this is clearly not the case here. To clarify

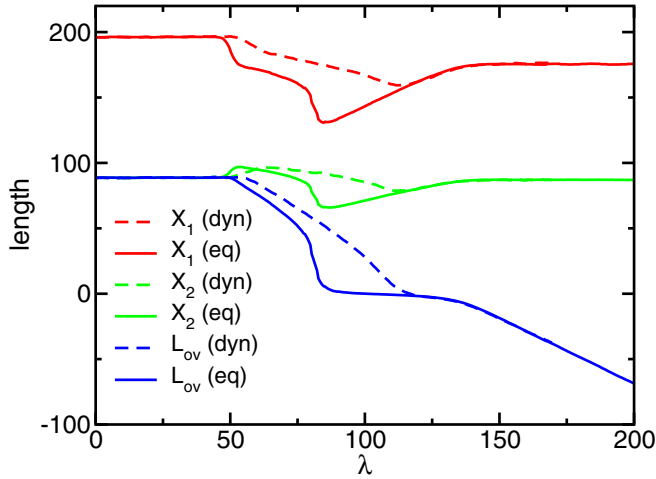


FIG. 9. Extension lengths and overlap distance vs λ . The graph compares the results obtained from equilibrium simulations with those obtained from a MC dynamics simulation for segregating polymers that initially overlap such that $\lambda = 0$. Results are shown for $N_1 = 400$, $N_2 = 200$, and $D = 4$.

this trend, we define τ^\dagger as the mean first-passage time for when the polymers reach a separation distance corresponding to the onset of the middle dynamical regime. The variation of τ^\dagger with N_2 is shown in the inset of Fig. 8(a). The variation is nonmonotonic and has a maximum τ^\dagger at $N_2 \approx 60$. The origin of this behavior stems from two competing trends. First, we note that τ^\dagger is approximately the time required for the system to reach the boundary between regimes I and II shown in Fig. 2. As noted in Sec. IV D this occurs at $\lambda \approx (X_1 - X_2)/2 = (X_1 - c_2 N_2)/2$. Thus, the separation distance at this boundary increases as N_2 decreases. In turn, this will tend to cause the time τ^\dagger to increase. On the other hand, decreasing N_2 also increases \mathcal{D}_2 and therefore also the relative diffusion rate $\mathcal{D}_1 + \mathcal{D}_2$. This effect will tend to decrease τ^\dagger . Evidently, at high N_2 the first effect dominates, while the second effect dominates at low N_2 , thus resulting in the maximum.

As noted above, the two transitions in the segregation kinetics occur near the I-II and III-IV regime boundaries of the corresponding free-energy functions. A close inspection reveals that the first transition in the kinetics occurs at a separation distance that is consistently larger than the I-II regime boundary. For example, for $N_2 = 150$, the transition occurs at $\lambda \approx 20$, while the I-II regime boundary is located at $\lambda \approx 14$. To understand this apparent discrepancy it is useful to examine once again the variation of the extension lengths and overlap distance with λ . In particular, we compare the behavior of these functions calculated during the segregation simulations with those calculated during the (equilibrium) calculations of the free-energy functions. Figure 9 shows the two sets of results calculated for a system with $N_1 = 400$, $N_2 = 200$, and $D = 4$. In regime I, the curves for each extension length calculated using the two methods overlap, and likewise for L_{ov} . This is also true in regime IV, where the polymers are no longer in physical contact. However, there is a significant difference between the two sets of results in the intermediate regimes. This indicates that segregation is not a quasistatic

process in this segregation stage, which explains the small discrepancies between the results of Figs. 8(a) and 8(b). For example, the transition associated with leaving the nesting state occurs at slightly a higher λ value in the results from the dynamics simulations relative to the equilibrium case, consistent with trends discussed above in relation to the behavior of the IMFPT.

Another noteworthy difference is the absence of any clear transition in the dynamics results associated with the regime II-III boundary of the free-energy function. The reason that the two sets of results diverge in this region is straightforward: it corresponds roughly to the regime where the driving force is greatest. Thus, the polymers are driven apart at a rate that is fast relative to that of the internal relaxation and out-of-equilibrium effects become significant. Once the driving force reduces to zero and unbiased diffusion dominates, then quasiequilibrium is restored.

We conclude with the following two observations concerning the relation between the segregation dynamics and the free-energy functions. First, the separation kinetics in the nesting regime, where the system is in quasiequilibrium, exhibits behavior consistent with the flat free-energy function for that regime. Second, a rapid increase in the separation rate occurs at λ very close to values corresponding to steep gradients in the free energy. Since out-of-equilibrium effects are present during this stage, the equilibrium free energy cannot be used in any quantitative analysis of the dynamics. However, the free energies do provide information on where such a rapid increase in the segregation rate is expected to occur.

V. CONCLUSIONS

In this study we have used MC simulations to study the physical behavior of two flexible hard-sphere polymer chains confined to infinitely long channels. Building on our previous studies of symmetric polymer or channel systems [19,21], we consider the effects of asymmetry in the polymer length. The main focus was the measurement and characterization of the variation of the free energy F with respect to the center-of-mass separation along the channel, λ . For the case where the polymer centers of mass are constrained to overlap, we also measure F with respect to extension length difference ζ . In addition, we used MC dynamics simulations to study the segregation dynamics of initially overlapping polymers.

A summary of the key findings is as follows. The free-energy functions $F(\lambda)$ exhibited the same four regimes [(I) nested, (II) partially overlapping, (III) compressed and nonoverlapping, and (IV) separated] as observed in our previous studies on polymer segregation [19,21]. In Fig. 7 we propose a regime map in which the state of the system is determined by the ratio of the polymer lengths, N_2/N_1 , and the scaled separation distance, $\lambda' \equiv \lambda/(N_1 + N_2)D^{-\beta}$. For sufficiently small N_2/N_1 , regime II disappears and the system passes directly from regime I to III as λ' increases. In regimes II, III and IV, the free-energy functions satisfy the scaling $F(\lambda) = (N_1 + N_2)D^{-\alpha} f[\lambda/(N_1 + N_2)D^{-\beta}]$, where $\alpha \approx 1.82$. and $\beta \approx 0.64$. In regime I, where the short polymer is nested inside the larger one, F is constant with respect to λ and satisfies $F \propto N_2 D^{-\beta}$, where $\beta \approx 0.64$. A simple theory constructed using de Gennes blob scaling and a previously

proposed model to describe the conformational behavior of overlapping polymers in channels [10] yields scaling behavior consistent with the observed behavior and predicts exponents of $\alpha = 1/\nu \approx 1.70$ and $\beta = 1 - 1/\nu \approx 0.70$. The small discrepancies arise from a combination of finite-size effects and deficiencies in the theoretical model of Ref. [10]. Regime I is also characterized by dynamics that are surprisingly similar to those expected for two noninteracting 1D random walkers undergoing unbiased diffusion. When the system crosses into regimes II and III, a rapid segregation occurs with out-of-equilibrium conformational behavior.

Our study has revealed a few intriguing effects in systems of polymers confined to channels related to the asymmetry in the contour lengths. The most notable are associated with the proposed “phase diagram” sketched in Fig. 7. In future work, it would be of interest to verify that the measured scaling of the free energy and the regime boundaries are preserved for much larger polymer systems and to develop theoretical models that yield more accurate predictions for the scaling exponents. In the future, we also plan to study the effects of other asymmetries, such as differences in polymer topology (e.g., ring and linear polymers), as well as asymmetries in the two lateral dimensions of the confining channel (e.g., using channels with rectangular cross sections).

It must be noted that this study and others like it are still very far removed from the long-term goal of accurately quantifying the degree to which entropic forces drive chromosome segregation in bacteria. Given the inherent complexity of such a biological system, the models are likely too simplistic for that ambitious goal, even with further refinements. A more realistic direction is modeling the behavior of “cleaner” *in vitro* systems such as DNA and other polymers confined to nanofabricated channels and cavities, as examined recently for example in Ref. [39]. We anticipate further such experimental examinations of systems of multiple polymers under confinement, the relevance of which is aligned more with development of nanofluidic devices for DNA manipulation and analysis. Accurate modeling of even these “simpler” systems is still challenging. At the very least, this requires using much longer, semiflexible chains that better describe polymers such as λ -DNA used in experiments. The type of asymmetry examined in this study may well be relevant to such future experiments.

ACKNOWLEDGMENTS

This work was supported by the Natural Sciences and Engineering Research Council of Canada (NSERC). We are grateful to Compute Canada and the Atlantic Computational Excellence Network (ACEnet) for use of their computational resources.

APPENDIX A: FREE ENERGY OF OVERLAPPING POLYMERS IN REGIME I

In this Appendix, we develop a theoretical model for the free-energy barrier height, ΔF , for channel-confined polymers of unequal chain length. The model is used to help understand the scaling properties of ΔF presented in Sec. IV B. We follow the approach taken by Minina and

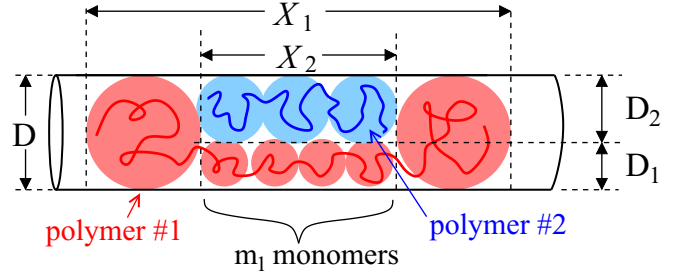


FIG. 10. Illustration of the various quantities described in the text of Appendix A for the case of $\zeta \equiv X_1 - X_2 > 0$. For the other case, where $\zeta \equiv X_1 - X_2 < 0$, the polymer 1 (red) would be nested inside of polymer 2 (blue).

Arnold in Refs. [16] and [17], which considered the special case of equal chain length.

Consider two polymers confined to a channel of diameter D in the case where polymer 2 of length N_2 is nested in a polymer 1 of length N_1 . Thus, the extension length difference satisfies $\zeta \equiv X_1 - X_2 > 0$. Employing the model of Jung *et al.* to describe overlapping polymers under confinement [10], the overlapping portions of the polymers effectively occupy separate virtual tubes of diameter D_1 and D_2 , both of which are less than D . We write $D_1 = D\sqrt{\xi}$ and $D_2 = D\sqrt{\xi_0 - \xi}$. In the case where lateral interpenetration is excluded, the sum of the cross sectional areas of the virtual tubes equals that of the real channel, which implies $\xi_0 = 1$. This choice was made in Refs. [16] and [17]. The quantity ξ is a measure of the fraction of the channel cross section effectively occupied by polymer 1, while $\xi_0 - \xi$ measures the same for polymer 2. Note that the extension length of polymer 2, X_2 , is also the distance along the channel over which the polymers overlap and, thus, the length of the two virtual tubes. The portion of polymer 1 outside this range is confined solely to the real tube of diameter D . Using the de Gennes blob theory (i.e., the extension length of polymer of length N confined to a tube of width D is $X \propto ND^{(v-1)/\nu}$), it follows that

$$m_1 D_1^{(v-1)/\nu} = N_2 D_2^{(v-1)/\nu}, \quad (\text{A1})$$

where $m_1 (\leq N_1)$ is the number of monomers of polymer 1 that lie within the span of 2, and where the scaling prefactors have canceled. The various quantities are illustrated in Fig. 10. Using the relation between virtual tube diameters and D introduced above, it is easily shown that

$$\xi(m_1/N_2) = \xi_0 \left[1 + \left(\frac{m_1}{N_2} \right)^{2\nu/(v-1)} \right]^{-1}. \quad (\text{A2})$$

Employing once again the de Gennes blob theory, the free energy of polymer 2 is

$$F_2 = N_2 D_2^{-1/\nu} = N_2 D^{-1/\nu} (\xi_0 - \xi)^{-1/2\nu}. \quad (\text{A3})$$

The free energy of polymer 1 has contributions from the overlapping and nonoverlapping (“overhang”) portions of the chain:

$$F_1 = (N_1 - m_1) D^{-1/\nu} + m_1 D^{-1/\nu} \xi^{-1/2\nu}. \quad (\text{A4})$$

Note that the scaling prefactors have been omitted from Eqs. (A3) and (A4).

It follows that the free energy in regime I relative to that of regime IV is

$$\Delta F = F_1(m_1) + F_2(m_1) - (N_1 + N_2)D^{-1/\nu}, \quad (\text{A5})$$

where the third term is the free energy in regime IV, where the polymers are sufficiently separated to not interact. From Eqs. (A2)–(A4), it follows that

$$\Delta F(m_1/N_2) = N_2 D^{-1/\nu} f(m_1/N_2; \xi_0), \quad (\text{A6})$$

where

$$f(x; \xi_0) = \xi(x)^{-1/2\nu} x + [\xi_0 - \xi(x)]^{-1/2\nu} - x - 1 \quad (\text{A7})$$

Neglecting fluctuations, the value of $x \equiv m_1/N_2$ is determined by minimization of f . Numerical determination of the minimum yields the linear relation of x and ξ with respect to ξ_0 :

$$\begin{aligned} x \equiv m_1/N_2 &= 0.79747 + 0.1\xi_0 \\ \xi &= -0.10903 + 0.53072\xi_0 \end{aligned} \quad (\text{A8})$$

in the range of $\xi_0 = 1$ –1.4. For the case of a nested polymer of length $N_2 = 200$, this corresponds to values ranging from $m_1 = 179.51$ and $\xi = 0.42348$ for $\xi_0 = 1$ to $m_1 = 187.51$ and $\xi = 0.63576$ for $\xi_0 = 1.4$. Note that $m_1 < N_2$ and $\xi > \xi_0 - \xi$. This implies that in the overlap regime the nested polymer is more longitudinally compressed and occupies a greater fraction of the cross-sectional area than that of the overlapping portion of the longer polymer.

APPENDIX B: NESTING FREE-ENERGY FUNCTION FOR $\lambda = 0$

Figure 5(a) shows the variation of the free energy with respect to the extension length difference, $\zeta = X_1 - X_2$, for two polymers of similar contour length and overlapping centers of mass (i.e., $\lambda = 0$). In this Appendix, we derive expressions that can be used to account for this behavior. As in Appendix A, we follow the approach taken by Minina and Arnold [16,17], who considered the special case of polymers of equal length. For simplicity, we consider only the case of $\xi_0 = 1$.

In Appendix A, we considered the case of $\zeta = X_1 - X_2 > 0$. There, the conformational free energy can be written as the sum

$$F(m_1) = F_1(m_1) + F_2(m_1), \quad (\text{B1})$$

where

$$F_1 = (N_1 - m_1)D^{-1/\nu} + m_1 D^{-1/\nu} \xi^{-1/2\nu} \quad (\text{B2})$$

and

$$F_2 = N_2 D_2^{-1/\nu} = N_2 D^{-1/\nu} (1 - \xi)^{-1/2\nu}. \quad (\text{B3})$$

In addition,

$$\xi(m_1) = \left[1 + \left(\frac{m_1}{N_2} \right)^{2\nu/(\nu-1)} \right]^{-1}. \quad (\text{B4})$$

Note these relations follow from Eqs. (A4), (A3), and (A2) for $\xi_0 = 1$. The difference in extension lengths, ζ , is the total span of the portion of polymer 1 located outside the region spanned by polymer 2. This is given by

$$\zeta(m_1) = (N_1 - m_1)D^{(\nu-1)/\nu}, \quad (\text{B5})$$

where we omit the prefactor. As both F and ζ are parameterized by m_1 the relationship between F and ζ is easily calculated.

Now consider the case where polymer 1 is nested within polymer 2, in which case $\zeta \equiv X_1 - X_2 < 0$. In addition, $m_1 = N_1$ and $m_2 (< N_2)$ are the number of monomers of each polymer within the span of polymer 1. Following the approach described above, it is easily shown that

$$\xi(m_2) = \xi_0 \left[1 + \left(\frac{N_1}{m_2} \right)^{2\nu/(\nu-1)} \right]^{-1}, \quad (\text{B6})$$

and the contributions to the free energy from both polymers are

$$F_1 = N_1 D^{-1/\nu} \xi^{-1/2\nu} \quad (\text{B7})$$

and

$$F_2 = (N_2 - m_2)D^{-1/\nu} + m_2 D^{-1/\nu} (1 - \xi)^{-1/2\nu}. \quad (\text{B8})$$

Thus, the total free energy,

$$F(m_2) = F_1(m_2) + F_2(m_2), \quad (\text{B9})$$

is a function of the quantity m_2 . Since $X_2 > X_1$, the extension length difference is the *negative* of the distance spanned by the portion of polymer 2 outside the range spanned by polymer 1:

$$\zeta(m_2) = -(N_2 - m_2)D^{(\nu-1)/\nu}. \quad (\text{B10})$$

Since both F and ζ are functions of the variable m_2 , the relationship between F and ζ is once again easily calculated.

Using these relations, which cover both regimes of $\zeta > 0$ and $\zeta < 0$, we have calculated $F(\zeta)$ for a system with $N_1 = 200$ and $D = 4$ for various values of N_2 . The results are shown in Fig. 5(b).

APPENDIX C: ADDITIONAL RESULTS ILLUSTRATING THE SCALING PROPERTIES OF THE FREE ENERGY

As described in Sec. IV A, the confined-polymer system is characterized by four scaling regimes. In Sec. IV D, we argue that the regimes are divided by boundaries that depend only the values of N_2/N_1 and $\lambda/(N_1 + N_2)D^{-\beta}$, where $\beta \approx 0.64$. This conclusion was made on the basis of the results of Fig. 6. The free-energy functions were shown to collapse to a universal curve when the axes were scaled such that $F' \equiv F/(N_1 + N_2)D^{-\alpha}$ is plotted as a function of $\lambda' \equiv \lambda/(N_1 + N_2)D^{-\beta}$, where $\alpha = 1.82$. Figure 6(a) and Fig. 6(b) show the data collapse for fixed $N_1 = 300$ and fixed $D = 6$ for various values of N_2 . Note that this collapse is only expected in regimes II–IV, and not for regime I, which accounts for the observed deviation from this scaling rule at low λ . Figure 6(b) and Fig. 6(d) show the data collapse for fixed $N_1 = 300$ and fixed $N_2 = 200$ for various values of D . As expected, the data collapse in Fig. 6(d) is valid for all regimes, including regime I, since N_2 is fixed.

Each of the free-energy functions presented in Fig. 6 corresponds to fixed $N_1 = 300$. The theoretical model predicts that the scaling boundaries in the λ' - F' plane do not depend on the specific value of N_1 . This is equivalent to the prediction that the scaled functions $F'(\lambda')$ are independent of N_1 . To test this invariance, we have calculated a collection of free-energy

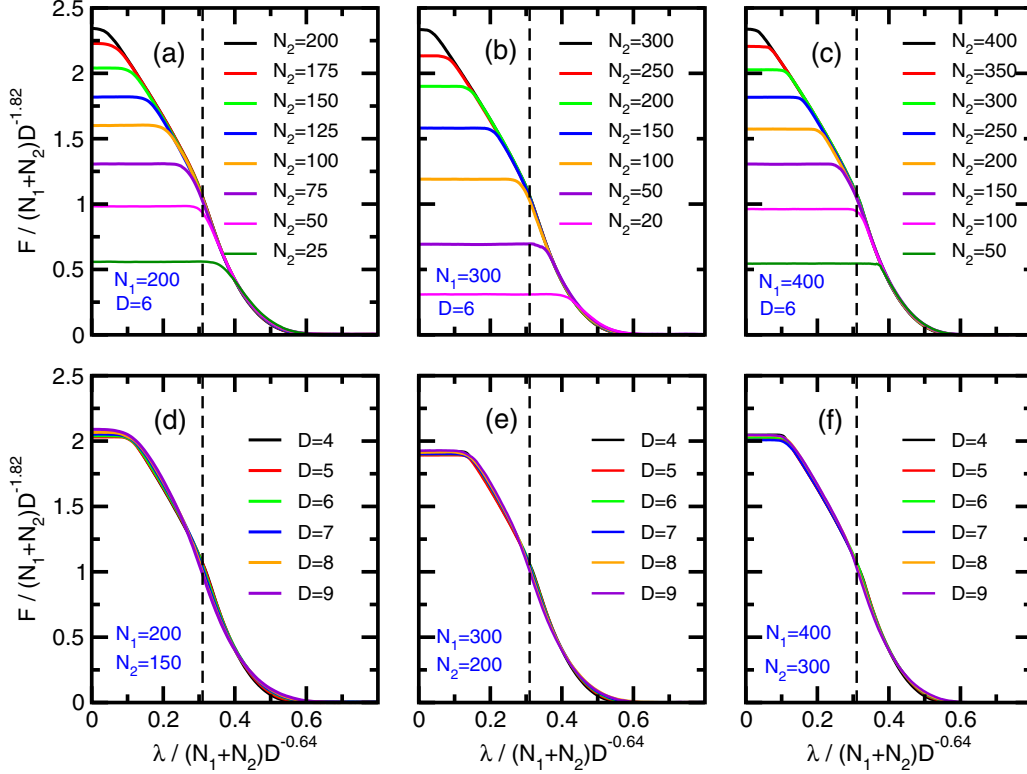


FIG. 11. Scaled free energy, $F/(N_1 + N_2)D^{-1.82}$ versus scaled polymer separation, $\lambda/(N_1 + N_2)D^{-0.64}$. Panels (a)–(c) each show results for fixed N_1 and fixed D for various values of N_2 . The results are arranged as follows: (a) $N_1 = 200$ and $D = 6$, (b) $N_1 = 300$ and $D = 6$, and (c) $N_1 = 400$ and $D = 6$. Panels (d)–(f) each show results for fixed N_1 and N_2 for various values of D . The results are arranged as follows: (d) $N_1 = 200$ and $N_2 = 150$, (e) $N_1 = 300$ and $N_2 = 200$, and (f) $N_1 = 400$ and $N_2 = 300$. The vertical dashed line in each panel marks the approximate boundary between regimes II and III.

functions for $N_1 = 200$ and $N_1 = 400$. Figure 11 below compares the scaled functions calculated for $N_1 = 200, 300$, and 400 . For each N_1 , we have varied N_2 at fixed D [Figs. 11(a)–11(c)], and have also varied D for fixed N_2 [Figs. 11(d)–11(f)]. The expected data collapse in the relevant regimes is observed. [Note that this does not include regime I for Figs. 11(a)–11(c)]. This result provides further evidence for the veracity of our claim regarding the regime boundaries.

APPENDIX D: SCALING OF $F(\lambda)$ IN REGIME II

In this Appendix, we develop a model to help understand the scaling properties of the free-energy function $F(\lambda)$ presented in Sec. IV D.

Consider the case of two partially overlapping polymers in regime II. The polymer lengths are N_1 and $N_2 \leq N_1$. Generally, the number of monomers of each polymer in the overlap region, m_1 and m_2 , need not be equal. However, we note from Fig. 4(a) that these are indeed very close to equal in this regime. Consequently, we define $m \equiv m_1 = m_2$. In addition, we choose the diameters of the virtual tubes to be $D_1 = D_2 = D/\sqrt{2}$. This corresponds to choosing $\xi = \frac{1}{2}$ and $\xi_0 = 1$ in Appendix A. The choice $\xi = \frac{1}{2}$ corresponds to the observation that $m_1 = m_2$. Choosing $\xi_0 = 1$ corresponds to not considering lateral interpenetration of the chains. We make this simplification since choosing instead $\xi_0 > 1$ changes only the

scaling prefactors and not the functional form of the scaling nor the values of the exponents.

The free energy of a partially overlapping chain is given by

$$F_1 = c_0(N_1 - m)D^{-1/\nu} + c_0(N_2 - m)D^{-1/\nu} + 2c_0m(D/\sqrt{2})^{-1/\nu}, \quad (D1)$$

where c_0 is a scaling constant. The first and second terms account for the parts of each polymer outside the overlap region. The third term is the contribution of the overlapping portion of the two polymers. The free energy of two polymers that are far apart (i.e., in regime IV) is given by

$$F_2 = c_0N_1D^{-1/\nu} + c_0N_2D^{-1/\nu}. \quad (D2)$$

The free energy in regime II relative to that of regime IV is thus

$$F = F_1 - F_2 = c'_0mD^{-1/\nu}, \quad (D3)$$

where $c'_0 \equiv (2^{1+1/2\nu} - 2)c_0$. It follows that

$$\frac{F}{(N_1 + N_2)D^{-1/\nu}} = c'_0 \left(\frac{m}{N_1 + N_2} \right) \quad (D4)$$

To determine the relationship between the free energy and λ , we need to find the relation between m and λ . For convenience, choose $z = 0$ to be the center of the overlap region, and define $z_1 (< 0)$ to be the center of mass of polymer 1 and

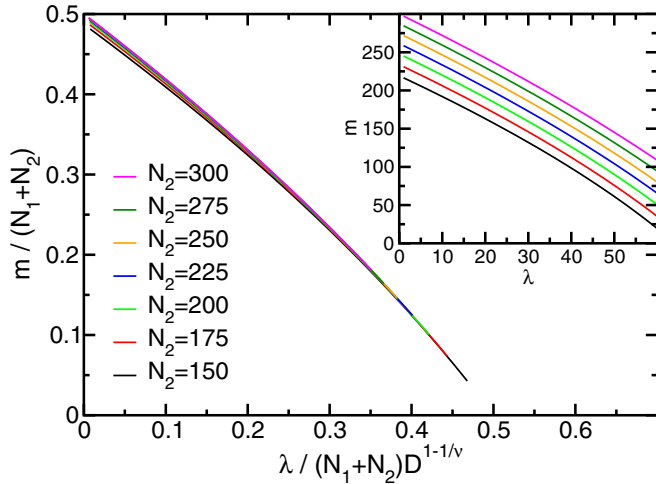


FIG. 12. Variation of $m/(N_1 + N_2)$ with $\lambda/(N_1 + N_2)D^{1-1/\nu}$ obtained by solving Eq. (D7) for the case of $N_1 = 300$ and $D = 6$. The inset shows the unscaled data.

$z_2 (> 0)$ to be the center of mass of polymer 2. It follows that

$$z_1 = \left(\frac{N_1 - m}{N_1} \right) \left(-\frac{1}{2}L_{ov} - \frac{1}{2}L_1 \right),$$

where L_1 is the extension length of polymer 1 outside of the overlap region. Note that $L_1 = c(N_1 - m)D^{1-1/\nu}$, where c is a constant, and also that $L_{ov} = c'mD^{1-1/\nu}$, where $c' \equiv 2^{-1/2+1/2\nu}c$. It can then be shown that

$$-2z_1/D^{1-1/\nu} = (c'' - c)m + cN_1 - c''m^2/N_1, \quad (D5)$$

where $c'' \equiv c' - c$. Likewise, it can be shown that z_2 is given by

$$2z_2/D^{1-1/\nu} = (c'' - c)m + cN_2 - c''m^2/N_2. \quad (D6)$$

From Eqs. (D5) and (D6) it follows that $\lambda \equiv z_2 - z_1$ satisfies:

$$\frac{\lambda}{(N_1 + N_2)D^{1-1/\nu}} = \Delta c \left(\frac{m}{N_1 + N_2} \right) + \frac{1}{2}c - \frac{1}{2}c'' \left(\frac{m}{N_1 + N_2} \right)^2 \frac{(N_1 + N_2)^2}{N_1 N_2}, \quad (D7)$$

where $\Delta c \equiv c'' - c$.

In the special case where $N_1 = N_2 \equiv N$, the factor $(N_1 + N_2)^2/N_2 N_2$ reduces to a constant, and the quadratic equation for the variable $m/(N_1 + N_2) \propto m/N$ can be solved to yield a relation of the form $m/N = u(\lambda/ND^{1-1/\nu})$, as noted in Ref. [21]. Substitution into Eq. (D4) then yields a scaling of $F(\lambda)$ consistent in form with that seen for the data presented in Sec. IV D; that is, $F(\lambda; N, D) = ND^{-1/\nu} f(\lambda/ND^{1-1/\nu})$, where $f(x) = u(x)$ in regime II. However, in the general case that $N_1 \neq N_2$, the resulting expression for $m/(N_1 + N_2)$ has a residual dependence on N_1 and N_2 beyond that implicit in the dependence on scaled variable $\lambda/(N_1 + N_2)D^{1-1/\nu}$. Consequently, the theoretical model does not exactly yield the scaling described by Eq. (3). In practice, however, the quantitative effect of the factor $(N_1 + N_2)^2/N_2 N_2$ is minimal. Figure 12 shows results for $m/(N_1 + N_2)$ vs $\lambda/(N_1 + N_2)D^{1-1/\nu}$ for $N_1 = 300$ and $D = 6$. The curves for various N_2 all come close to collapsing to a universal curve. The greatest deviation occurs for low λ for cases where the system has transitioned into regime I, where these results are not relevant. Similar results were obtained for other values of N_1 . We conclude that the theoretical model produces results that come very close to yielding the predicted scaling of Eq. (3) in regime II.

-
- [1] A. Y. Grosberg, P. G. Khalatur, and A. R. Khokhlov, *Makromol. Chem. Rapid Comm.* **3**, 709 (1982).
- [2] J. Dautenhahn and C. K. Hall, *Macromolecules* **27**, 5399 (1994).
- [3] M. Daoud and P. De Gennes, *J. Phys. (Paris)* **38**, 85 (1977).
- [4] S. Jun and B. Mulder, *Proc. Natl. Acad. Sci. USA* **103**, 12388 (2006).
- [5] I. Teraoka and Y. Wang, *Polymer* **45**, 3835 (2004).
- [6] S. Jun, A. Arnold, and B.-Y. Ha, *Phys. Rev. Lett.* **98**, 128303 (2007).
- [7] A. Arnold and S. Jun, *Phys. Rev. E* **76**, 031901 (2007).
- [8] J. L. Jacobsen, *Phys. Rev. E* **82**, 051802 (2010).
- [9] Y. Jung and B.-Y. Ha, *Phys. Rev. E* **82**, 051926 (2010).
- [10] Y. Jung, C. Jeon, J. Kim, H. Jeong, S. Jun, and B.-Y. Ha, *Soft Matter* **8**, 2095 (2012).
- [11] Y. Jung, J. Kim, S. Jun, and B.-Y. Ha, *Macromolecules* **45**, 3256 (2012).
- [12] Y. Liu and B. Chakraborty, *Phys. Biol.* **9**, 066005 (2012).
- [13] J. Dorier and A. Stasiak, *Nucleic Acids Res.* **41**, 6808 (2013).
- [14] D. Račko and P. Cifra, *J. Chem. Phys.* **138**, 184904 (2013).
- [15] J. Shin, A. G. Cherstvy, and R. Metzler, *New J. Phys.* **16**, 053047 (2014).
- [16] E. Minina and A. Arnold, *Soft Matter* **10**, 5836 (2014).
- [17] E. Minina and A. Arnold, *Macromolecules* **48**, 4998 (2015).
- [18] Y. Chen, W. Yu, J. Wang, and K. Luo, *J. Chem. Phys.* **143**, 134904 (2015).
- [19] J. M. Polson and L. G. Montgomery, *J. Chem. Phys.* **141**, 164902 (2014).
- [20] Y. Du, H. Jiang, and Z. Hou, *J. Chem. Phys.* **149**, 244906 (2018).
- [21] J. M. Polson and D. R.-M. Kerry, *Soft Matter* **14**, 6360 (2018).
- [22] W. Nowicki, *J. Chem. Phys.* **150**, 014902 (2019).
- [23] W. Nowicki, *J. Mol. Model.* **25**, 269 (2019).
- [24] S. Jun and A. Wright, *Nat. Rev. Microbiol.* **8**, 600 (2010).
- [25] B. Di Ventura, B. Knecht, H. Andreas, W. J. Godinez, M. Fritsche, K. Rohr, W. Nickel, D. W. Heermann, and V. Sourjik, *Mol. Syst. Biol.* **9**, 686 (2013).
- [26] B. Youngren, H. J. Nielsen, S. Jun, and S. Austin, *Genes Dev.* **28**, 71 (2014).

- [27] J. Männik, D. E. Castillo, D. Yang, G. Siopsis, and J. Männik, *Nucleic Acids Res.* **44**, 1216 (2016).
- [28] A. Badrinarayanan, T. B. Le, and M. T. Laub, *Ann. Rev. Cell Devel Biol.* **31**, 171 (2015).
- [29] M. Fritsche, S. Li, D. W. Heermann, and P. A. Wiggins, *Nucleic Acids Res.* **40**, 972 (2011).
- [30] V. G. Benza, B. Bassetti, K. D. Dorfman, V. F. Scolari, K. Bromek, P. Cicuta, and M. C. Lagomarsino, *Rep. Prog. Phys.* **75**, 076602 (2012).
- [31] N. H. Yazdi, C. C. Guet, R. C. Johnson, and J. F. Marko, *Mol. Microbiol.* **86**, 1318 (2012).
- [32] J. K. Fisher, A. Bourniquel, G. Witz, B. Weiner, M. Prentiss, and N. Kleckner, *Cell* **153**, 882 (2013).
- [33] N. J. Kuwada, K. C. Cheveralls, B. Traxler, and P. A. Wiggins, *Nucleic Acids Res.* **41**, 7370 (2013).
- [34] J. A. Cass, N. J. Kuwada, B. Traxler, and P. A. Wiggins, *Biophys. J.* **110**, 2597 (2016).
- [35] L. J. Wu, S. Lee, S. Park, L. Eland, A. Wipat, S. Holden, and J. Errington, *Nat. Commun.* **11**, 4149 (2020).
- [36] N. El Najjar, D. Geisel, F. Schmidt, S. Dersch, B. Mayer, R. Hartmann, B. Eckhardt, P. Lenz, and P. L. Graumann, *mSphere* **5**, e00255-20 (2020).
- [37] A. Japaridze, C. Gogou, J. W. Kerssemakers, H. M. Nguyen, and C. Dekker, *Nat. Commun.* **11**, 3109 (2020).
- [38] A. Hofmann, J. Mäkelä, D. J. Sherratt, D. Heermann, and S. M. Murray, *Elife* **8**, e46564 (2019).
- [39] X. Capaldi, Z. Liu, Y. Zhang, L. Zeng, R. Reyes-Lamothe, and W. Reisner, *Soft Matter* **14**, 8455 (2018).
- [40] J. Han and H. G. Craighead, *Science* **288**, 1026 (2000).
- [41] S. W. P. Turner, M. Cabodi, and H. G. Craighead, *Phys. Rev. Lett.* **88**, 128103 (2002).
- [42] D. Frenkel and B. Smit, *Understanding Molecular Simulation: From Algorithms to Applications*, 2nd ed. (Academic Press, London, 2002), Chap. 7.
- [43] D. P. Landau and K. Binder, *A Guide to Monte-Carlo Simulations in Statistical Physics*, 3rd ed. (Cambridge University Press, Cambridge, 2009), Chap. 6.
- [44] J. M. Polson and A. C. McCaffrey, *J. Chem. Phys.* **138**, 174902 (2013).
- [45] H. W. de Haan and G. W. Slater, *J. Chem. Phys.* **134**, 154905 (2011).
- [46] H. W. de Haan and G. W. Slater, *J. Chem. Phys.* **136**, 204902 (2012).
- [47] P. de Gennes, *Scaling Concepts in Polymer Physics* (Cornell University Press, Ithica, NY, 1979).
- [48] J. Kim, C. Jeon, H. Jeong, Y. Jung, and B.-Y. Ha, *Soft Matter* **9**, 6142 (2013).
- [49] S. Jun, D. Thirumalai, and B.-Y. Ha, *Phys. Rev. Lett.* **101**, 138101 (2008).
- [50] S. Redner, *A Guide to First-Passage Processes* (Cambridge University Press, Cambridge, 2001).